

Elucidating the nature and role of Cu species in enhanced catalytic carbonylation of dimethyl ether over Cu/H-MOR

Supporting Information

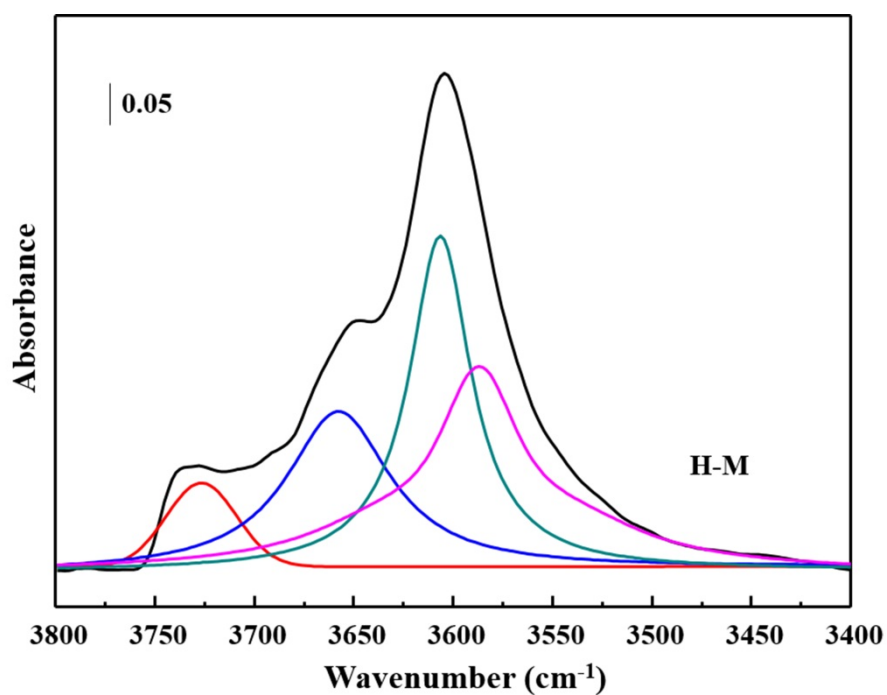


Fig. S1 FTIR spectra in the O–H stretching region of H-M sample (-) and deconvoluted bands corresponding to H⁺ in 8-MR (-) and 12-MR (-), extra-framework Al–OH (-) and Si–OH (-).

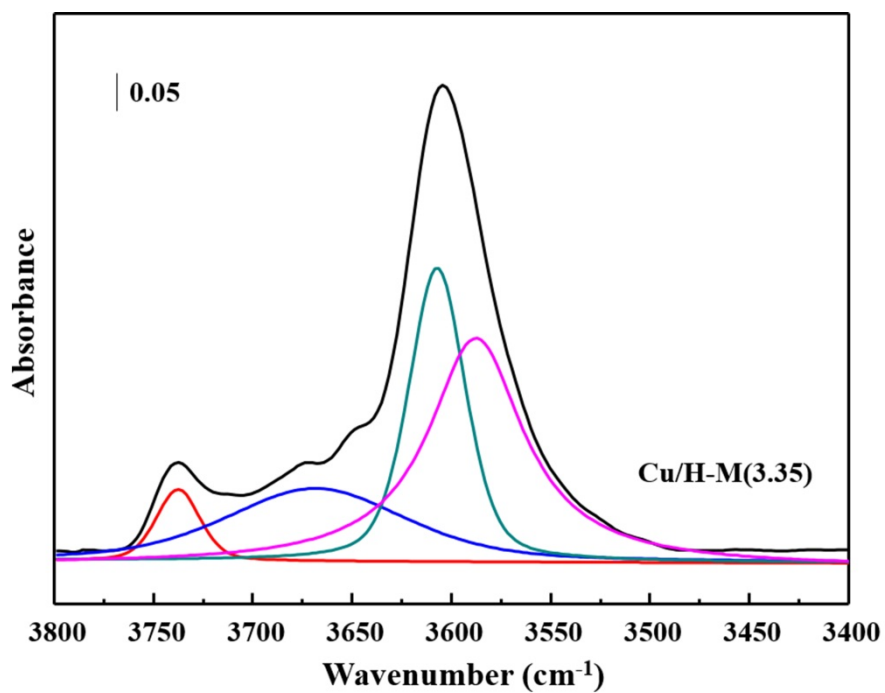


Fig. S2 FTIR spectra in the O–H stretching region of un-reduced Cu/H-M(3.35) sample (-) and deconvoluted bands corresponding to H⁺ in 8-MR (-) and 12-MR (-), extra-framework Al–OH (-) and Si–OH (-).

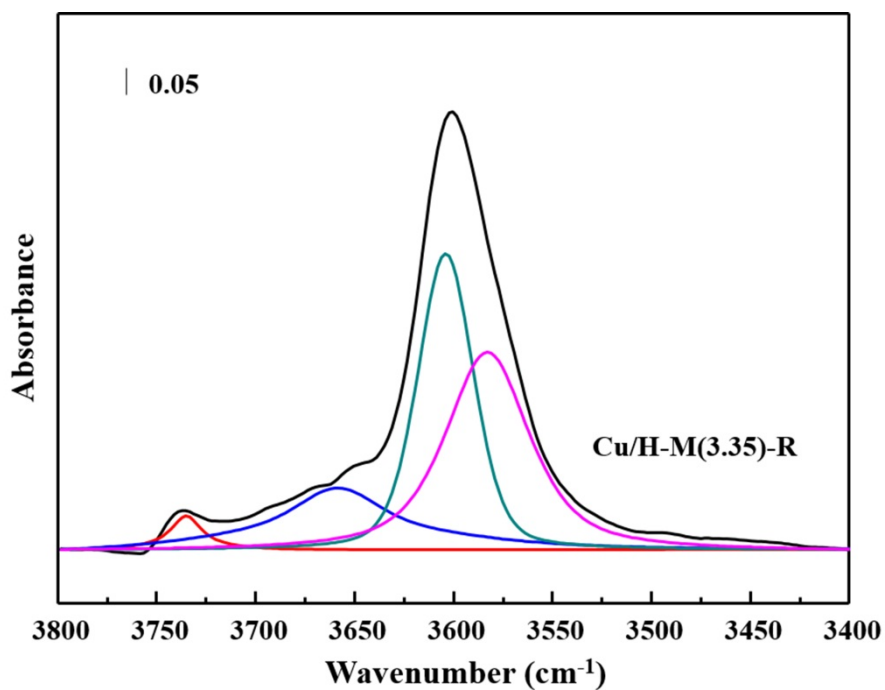


Fig. S3 FTIR spectra in the O–H stretching region of reduced Cu/H-M(3.35) sample (-) and deconvoluted bands corresponding to H⁺ in 8-MR (-) and 12-MR (-), extra-framework Al–OH (-) and Si–OH (-).

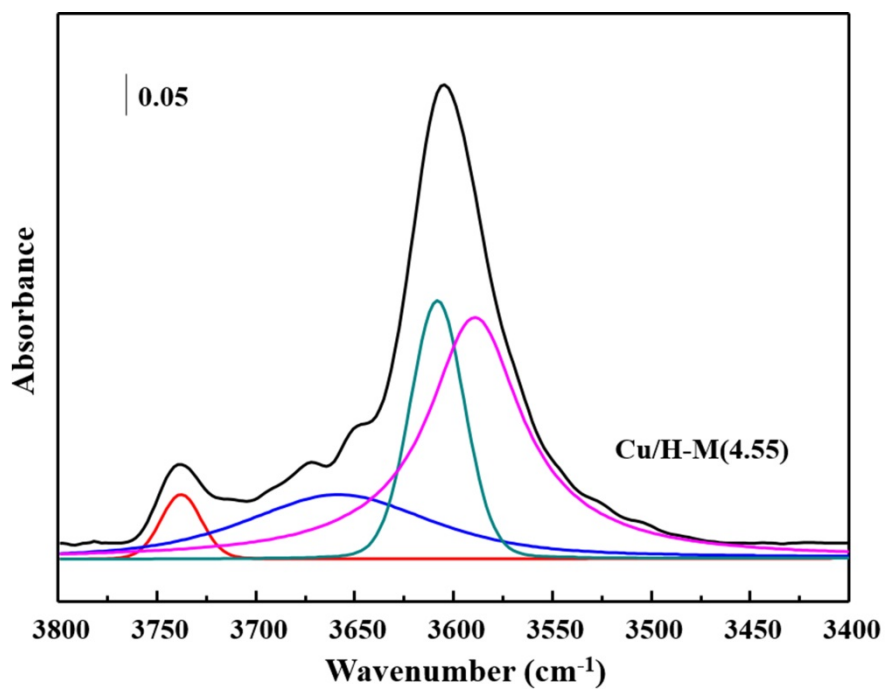


Fig. S4 FTIR spectra in the O–H stretching region of un-reduced Cu/H-M(4.55) sample (-) and deconvoluted bands corresponding to H⁺ in 8-MR (-) and 12-MR (-), extra-framework Al–OH (-) and Si–OH (-).

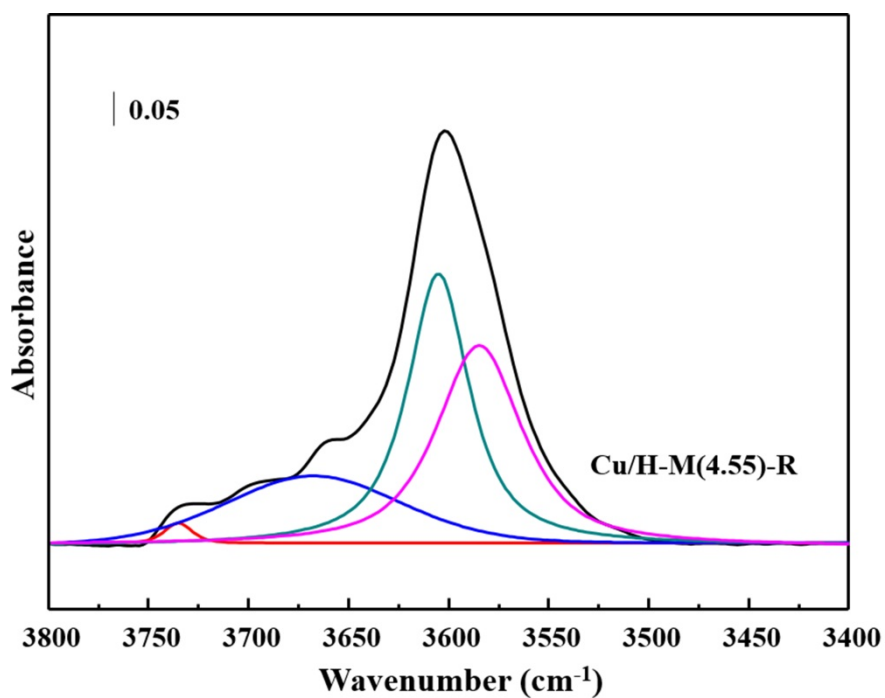


Fig. S5 FTIR spectra in the O–H stretching region of reduced Cu/H-M(4.55) sample (-) and deconvoluted bands corresponding to H⁺ in 8-MR (-) and 12-MR (-), extra-framework Al–OH (-) and Si–OH (-).

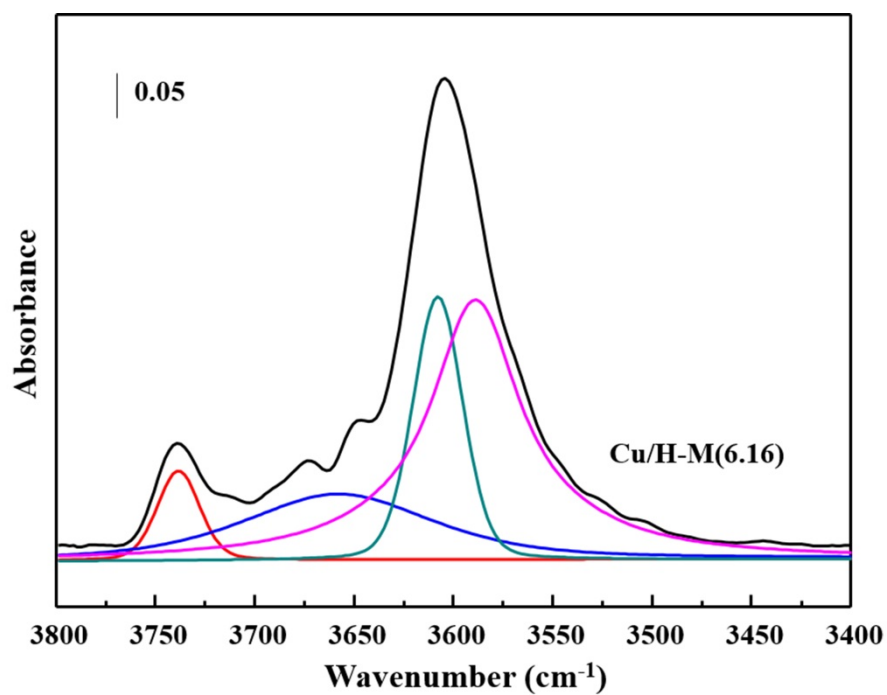


Fig. S6 FTIR spectra in the O–H stretching region of un-reduced Cu/H-M(6.16) sample (-) and deconvoluted bands corresponding to H⁺ in 8-MR (-) and 12-MR (-), extra-framework Al–OH (-) and Si–OH (-).

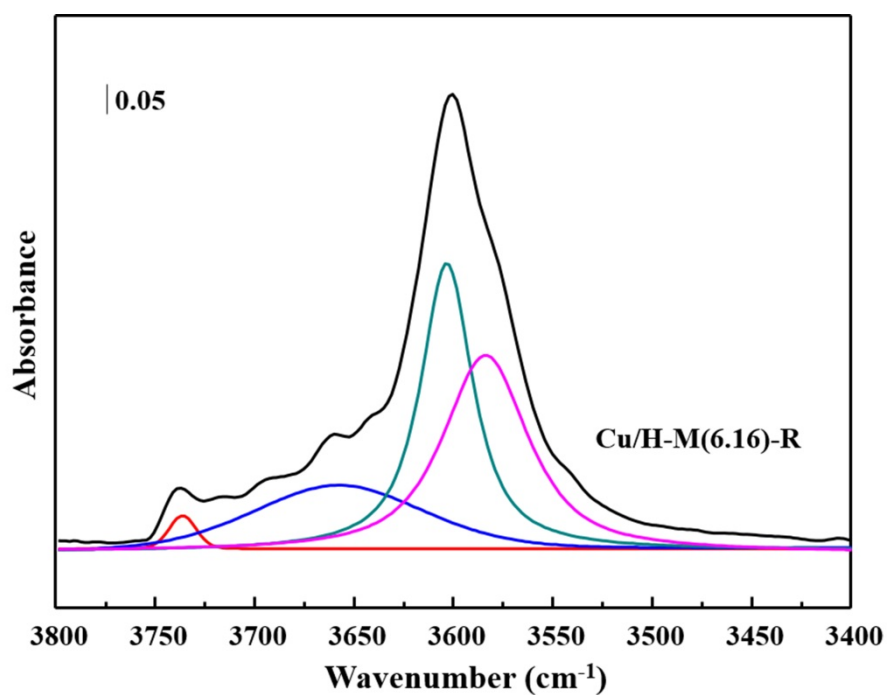


Fig. S7 FTIR spectra in the O–H stretching region of reduced Cu/H-M(6.16) sample (-) and deconvoluted bands corresponding to H⁺ in 8-MR (-) and 12-MR (-), extra-framework Al–OH (-) and Si–OH (-).

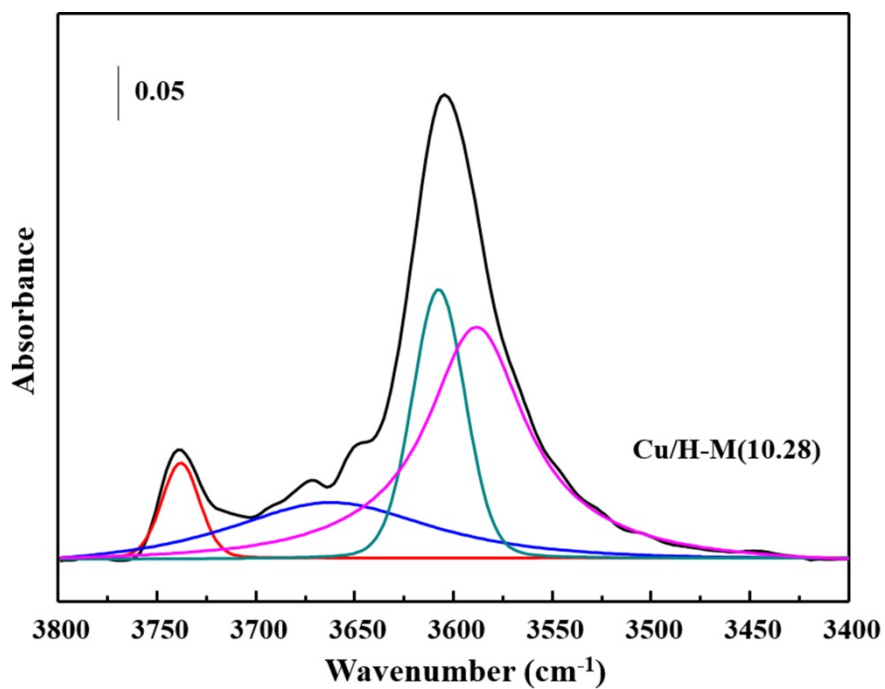


Fig. S8 FTIR spectra in the O–H stretching region of unreduced Cu/H-M(10.28) sample (-) and deconvoluted bands corresponding to H⁺ in 8-MR (-) and 12-MR (-), extra-framework Al–OH (-) and Si–OH (-).

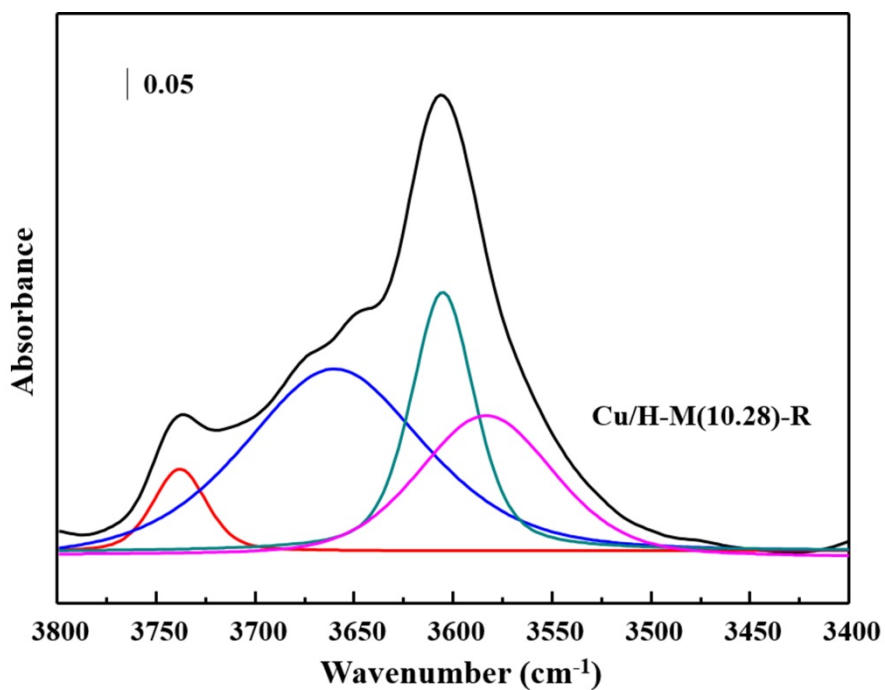


Fig. S9 FTIR spectra in the O–H stretching region of reduced Cu/H-M(10.28) sample (-) and deconvoluted bands corresponding to H⁺ in 8-MR (-) and 12-MR (-), extra-framework Al–OH (-) and Si–OH (-).

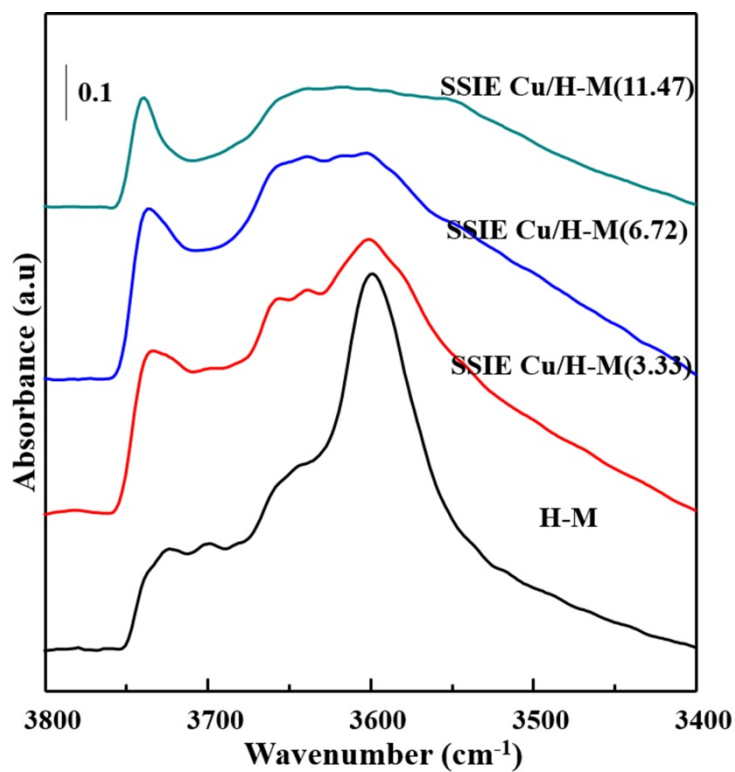


Fig. S10 FTIR spectra in the O-H stretching region of H-MOR and SSIE Cu/H-M(x) samples

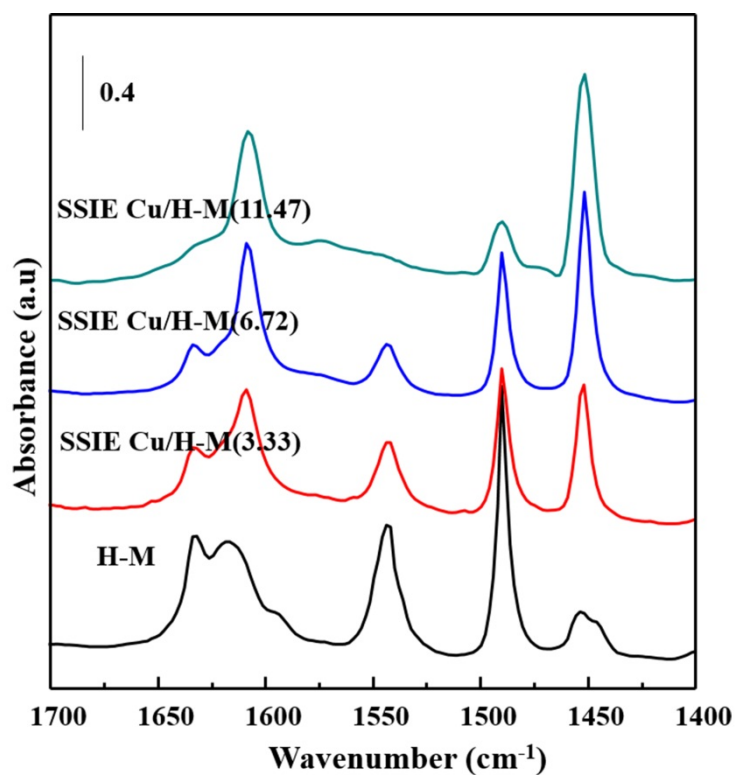


Fig. S11 FTIR spectra of pyridine adsorbed on H-MOR and SSIE Cu/H-M(x) samples

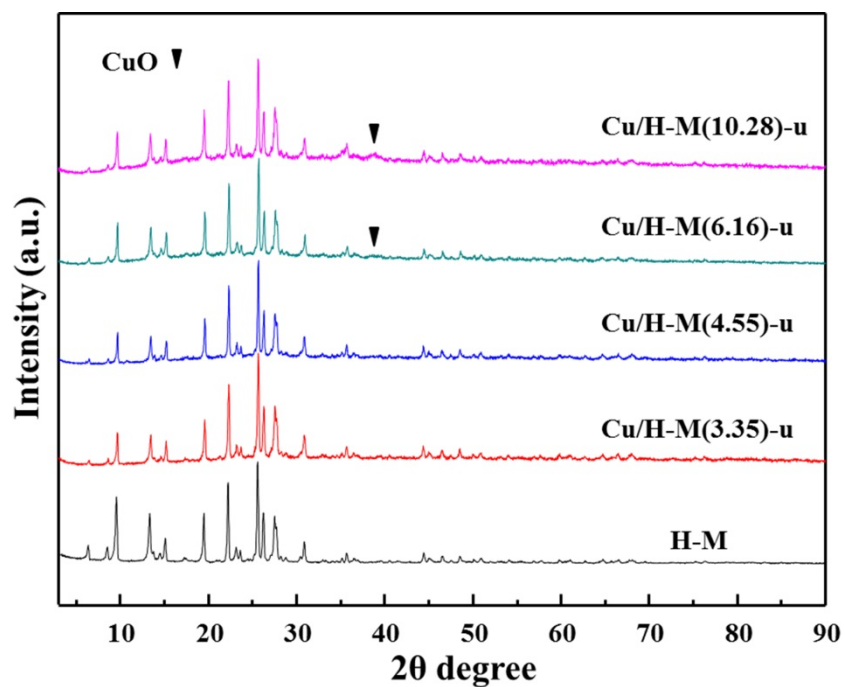


Fig. S12 XRD patterns of the unreduced Cu/H-M(x) samples. (-u: unreduced)

XRD patterns of the unreduced Cu/H-M(x) samples reveal that no bulk Cu species can be detected at low Cu loading. With the increase of Cu loading, a slight characteristic peak at 38.9° attributed to CuO can be distinguished, indicating the presence of CuO aggregates.

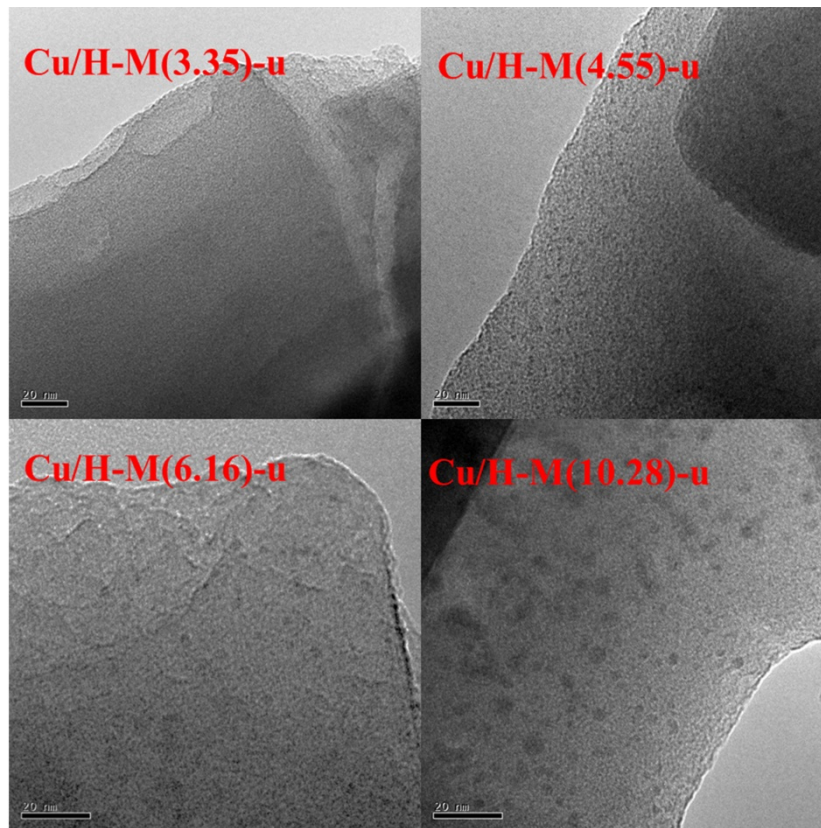


Fig. S13 TEM images of the unreduced Cu/H-M(x) samples. (-u: unreduced)

TEM images of the unreduced Cu/H-M(x) samples present that few Cu oxides particles can be found for Cu/H-M(3.35) sample, while the number and size of Cu oxides particles increase with the increase of Cu loading.

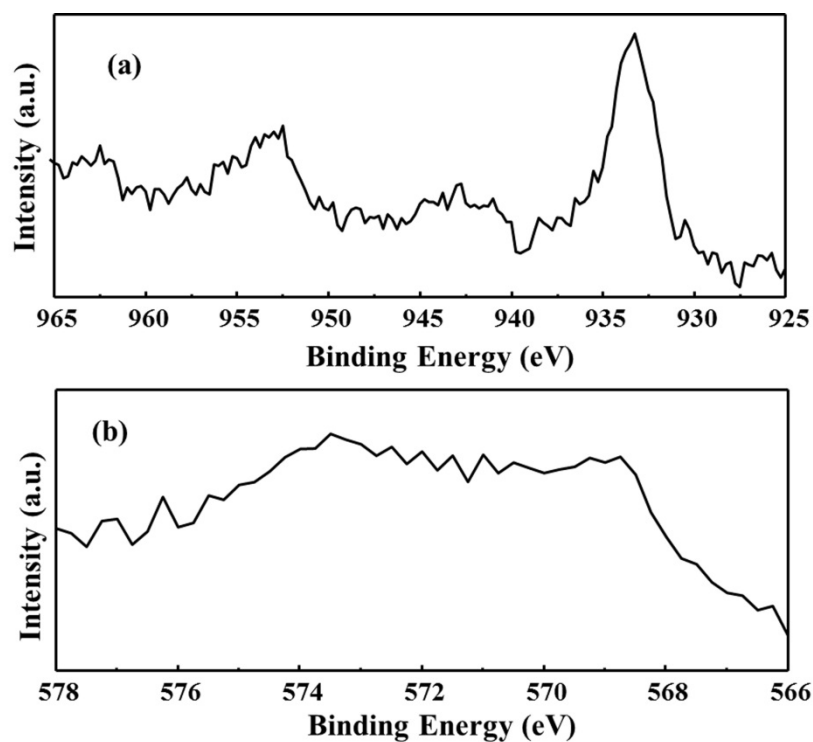


Fig. S14 Cu 2p XPS and Cu LMM XAES spectra of the unreduced Cu/H-M(4.55) sample. (a: Cu 2p XPS spectrum, b: Cu LMM XAES spectrum)

The satellite peaks in Cu 2p XPS spectrum at about 942.7 (Cu 2p 3/2) and 962.5 eV (Cu 2p 1/2 for CuO) proves the existence of divalent Cu, and the broad peak in Cu LMM XAES spectrum demonstrates the coexistence of multiple valence state of Cu species.

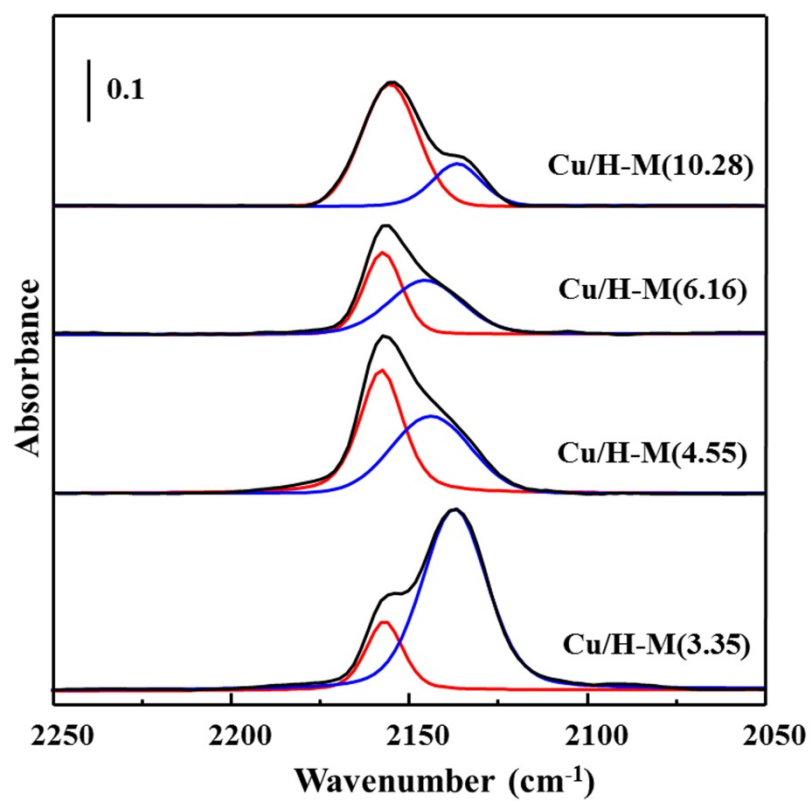


Fig. S15 FTIR spectra of CO adsorption for reduced Cu/H-M(x) samples (-) and deconvoluted bands corresponding to Cu⁺ in 8-MR (-) and 12-MR (-) channels.

All of the as-prepared Cu/H-M(x) samples are reduced and re-evaluated under the conditions as mentioned in the text, and then cooled down to room temperature in N₂ flow after 8 h reaction. The spent catalysts are transferred and sealed in a glove box and characterized by XRD, TEM as well as CO-adsorption IR.

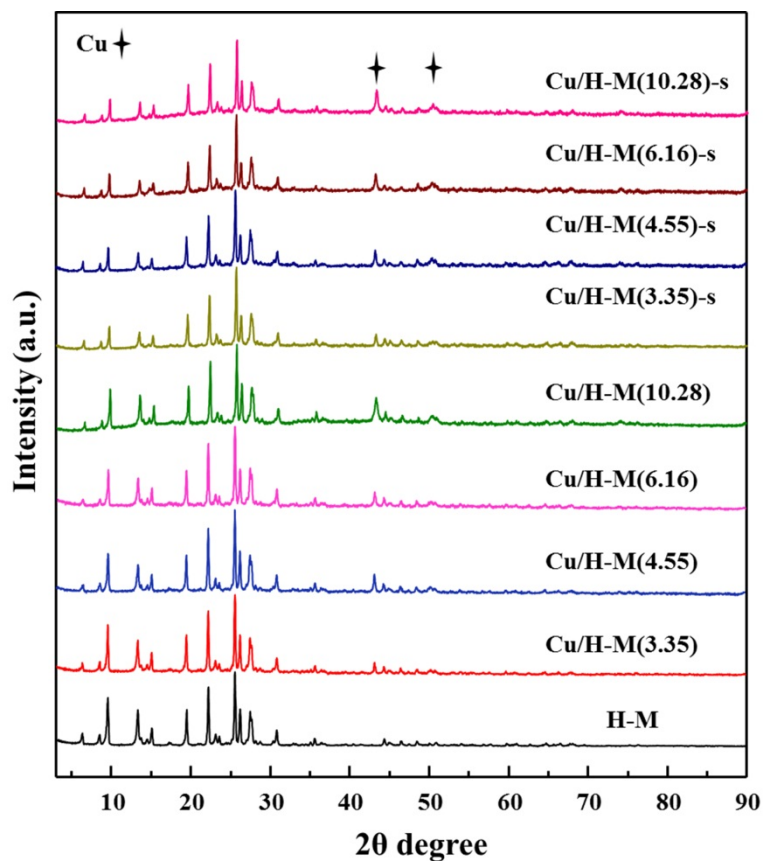


Fig. S16 XRD patterns of the reduced and spent Cu/H-M(x) samples. (-s: spent)

As shown in Fig. S16, zeolitic framework of the spent Cu/H-M(x) catalysts is well maintained. The characteristic peaks at 43.3° and 50.5° assigned to Cu⁰ exhibit few differences compared with the reduced Cu/H-M(x) samples.

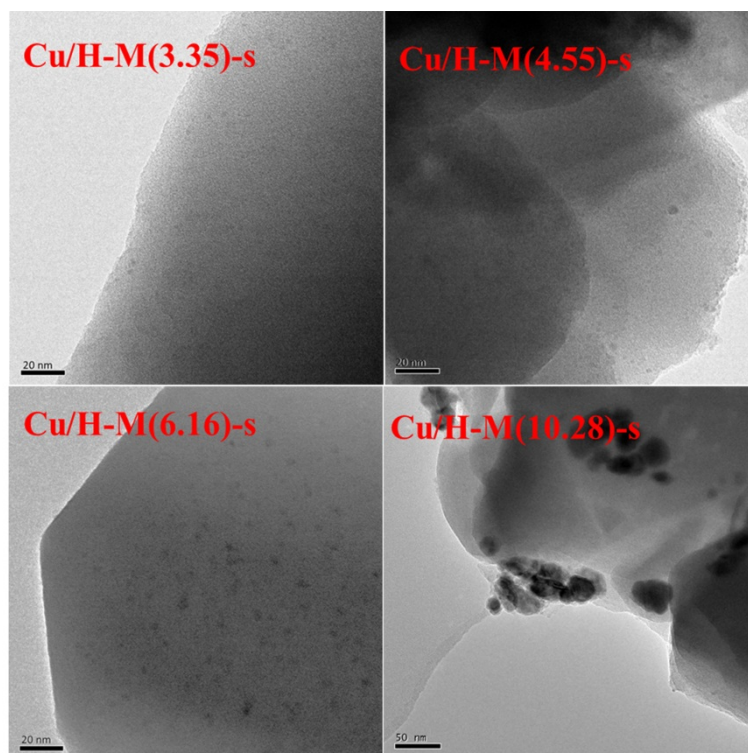


Fig. S17 TEM images of the spent Cu/H-M(x) samples. (-s: spent)

The distribution and particle size of Cu⁰ particles for the spent Cu/H-M(x) samples are similar to that for the reduced Cu/H-M(x) samples (shown in Fig. 3 of the paper).

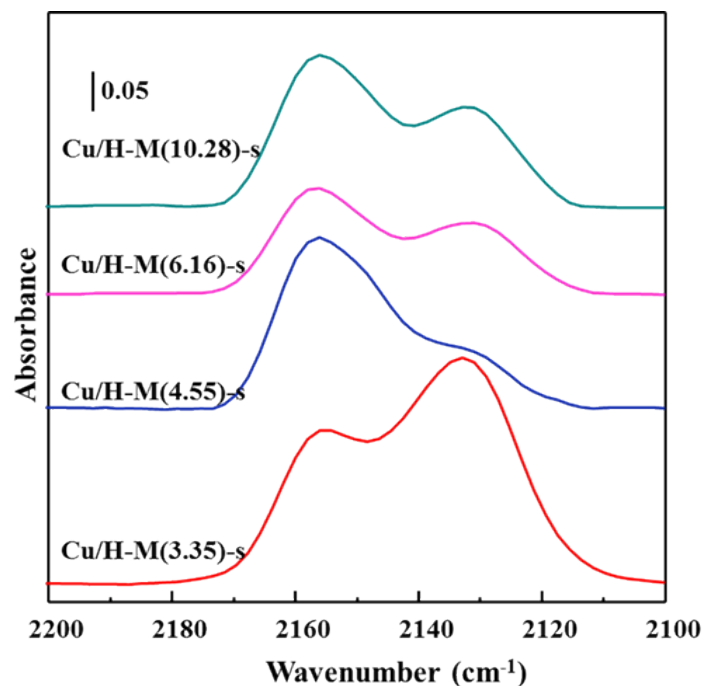


Fig. S18 FTIR spectra of CO adsorption for spent Cu/H-M(x) samples. (-s: spent)

The *in situ* DRIFTS of CO adsorption is used to provide detailed information of Cu^+ species in spent Cu/H-M(x) samples. As the presence of adsorbed methyl groups leads to a consumption of CO on the spent catalysts, we extend the adsorption time of samples to 4 h in CO flow. And the spectra are collected after He purging for 2 h until the intensities of bands are not changed. The similarity of the IR bands in the range of $2100 \sim 2200 \text{ cm}^{-1}$ between the fresh catalysts (shown in Fig. 8 of the paper) and used ones indicates that the location and amount of Cu^+ remain almost unchanged. Hence, we suggest that Cu species are relatively stable during reaction.

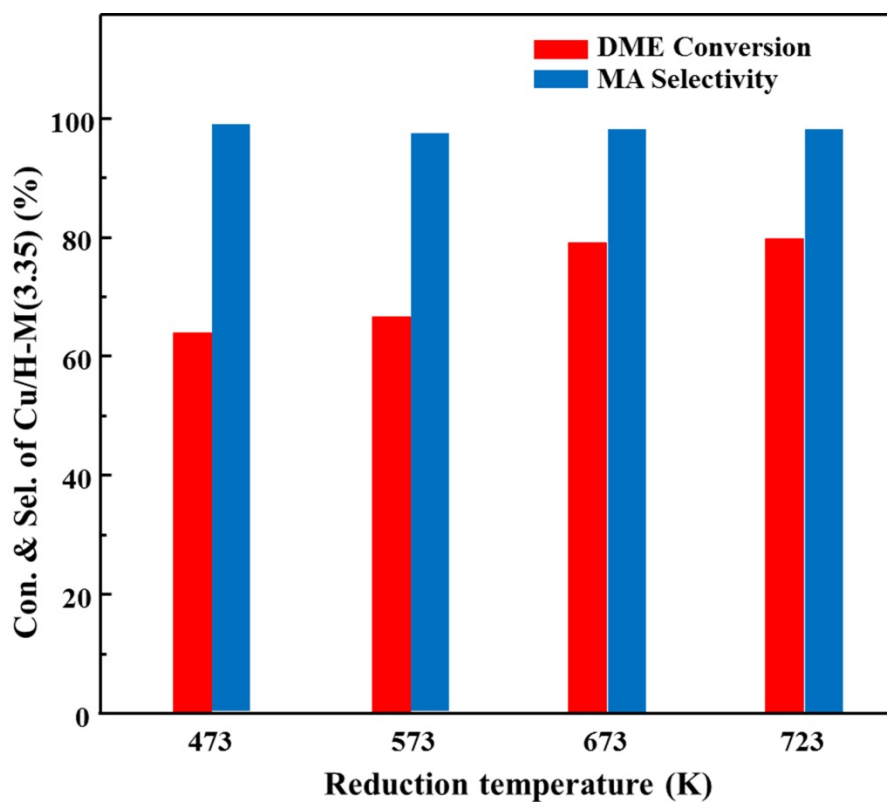


Fig. S19 DME conversion and MA selectivity for Cu/H-M(3.35) sample under different reduction temperature. (Reaction condition: DME/CO = 1/47, 473 K, 1.5 MPa, 4500 h⁻¹, 1.2 g_{cat}).

In order to testify the acceleration effect of Cu⁰, the influence of different reduction temperature for Cu/H-M(3.35) sample are investigated. With increase of reduction temperature from 473 K to 673 K, the activity is apparently improved with the similar selectivity. It also supports our conclusion strongly.